

GRIT: Graph-Regularized Logit Refinement for Zero-shot Cell Type Annotation

Tianxiang Hu

Zhejiang University

Hangzhou, China

tianxiang.23@intl.zju.edu.cn

Chenyi Zhou

Zhejiang University

Hangzhou, China

chenyi.22@intl.zju.edu.cn

Jiaxiang Liu

Guangdong Institute of Intelligence

Science and Technology

Hengqin, China

liujiaxiang@gdiist.cn

Jiongxin Wang

Zhejiang University

Hangzhou, China

jiongxin.23@intl.zju.edu.cn

Ruizhe Chen

Zhejiang University

Hangzhou, China

ruizhe.21@intl.zju.edu.cn

Haoxiang Xia

Zhejiang University

Hangzhou, China

haoxiang.22@intl.zju.edu.cn

Gaoang Wang

Zhejiang University

Hangzhou, China

gaoangwang@intl.zju.edu.cn

Jian Wu

Zhejiang University

Hangzhou, China

jianwu@intl.zju.edu.cn

Zuozhu Liu

Zhejiang University

Hangzhou, China

zuozhuliu@intl.zju.edu.cn

Abstract

Cell type annotation is a fundamental step in the analysis of single-cell RNA sequencing (scRNA-seq) data. In practice, human experts often rely on the structure revealed by principal component analysis (PCA) followed by k -nearest neighbor (k -NN) graph construction to guide annotation. While effective, this process is labor-intensive and does not scale to large datasets. Recent advances in CLIP-style models offer a promising path toward automating cell type annotation. By aligning scRNA-seq profiles with natural language descriptions, models like LangCell enable zero-shot annotation. While LangCell demonstrates decent zero-shot performance, its predictions remain suboptimal. In this paper, we propose a principled inference-time paradigm for zero-shot cell type annotation (GRIT) which bridges the scalability of pre-trained foundation models with the structural robustness relied upon in human expert annotation workflows. Specifically, we enforce local consistency of the zero-shot CLIP logits over the task-specific PCA-based k -NN graph. We evaluate our approach on 14 annotated human scRNA-seq datasets from 4 distinct studies, spanning 11 organs and over 200,000 single cells. Our method consistently improves zero-shot annotation accuracy, achieving accuracy gains of up to 10%. Further analysis showcase the mechanism by which GRIT effectively propagates correct signals through the graph, pulling back mislabeled cells toward more accurate predictions. The method is training-free, model-agnostic, and serves as a simple yet effective plug-in for enhancing zero-shot cell type annotation.

Permission to make digital or hard copies of all or part of this work for personal or classroom use is granted without fee provided that copies are not made or distributed for profit or commercial advantage and that copies bear this notice and the full citation on the first page. Copyrights for components of this work owned by others than the author(s) must be honored. Abstracting with credit is permitted. To copy otherwise, or republish, to post on servers or to redistribute to lists, requires prior specific permission and/or a fee. Request permissions from permissions@acm.org.

Conference'17, Washington, DC, USA

© 2026 Copyright held by the owner/author(s). Publication rights licensed to ACM.

ACM ISBN 978-x-xxxx-xxxx-x/YY/MM

<https://doi.org/10.1145/nnnnnnnnnnnnnnn>

Keywords

Cell type annotation, scRNA-seq, CLIP, Zero-shot classification

ACM Reference Format:

Tianxiang Hu, Chenyi Zhou, Jiaxiang Liu, Jiongxin Wang, Ruizhe Chen, Haoxiang Xia, Gaoang Wang, Jian Wu, and Zuozhu Liu. 2026. GRIT: Graph-Regularized Logit Refinement for Zero-shot Cell Type Annotation. In . ACM, New York, NY, USA, 10 pages. <https://doi.org/10.1145/nnnnnnnnnnnnnnn>

1 Introduction

Single-cell RNA sequencing (scRNA-seq) technologies have enabled high-resolution profiling of cellular heterogeneity across diverse tissues and biological conditions [16, 29]. A critical step in the analysis pipeline is cell type annotation—assigning biologically meaningful labels to individual cells—which forms the basis for downstream interpretation. Traditionally, this process is performed through a semi-automatic workflow [3, 4, 13, 27, 30, 32], combining dimensionality reduction (e.g., principal component analysis), clustering algorithms (e.g., Leiden or Louvain), and manual inspection of marker gene expression. However, this approach is time-consuming and increasingly impractical as scRNA-seq datasets grow in size and complexity.

Recent advances in deep learning have enabled the development of powerful representation learning frameworks for scRNA-seq data. Models such as scBERT [42], scGPT [7], Geneformer [8], and scFoundation [11] are pretrained on millions of single-cell profiles and support transfer learning for a wide range of downstream tasks. These foundation models offer a unified and scalable approach to encoding single-cell gene expression into informative embeddings using general-purpose neural architectures. Building on this foundation, LangCell [45] adopts Geneformer—a high-performing single-cell foundation model—as its cell encoder within a CLIP-style framework that aligns single-cell embeddings with natural language descriptions of cell identities. By training on paired scRNA-seq profiles and cell-type text annotations, LangCell uniquely enables zero-shot cell type annotation. Given the success of CLIP-style and

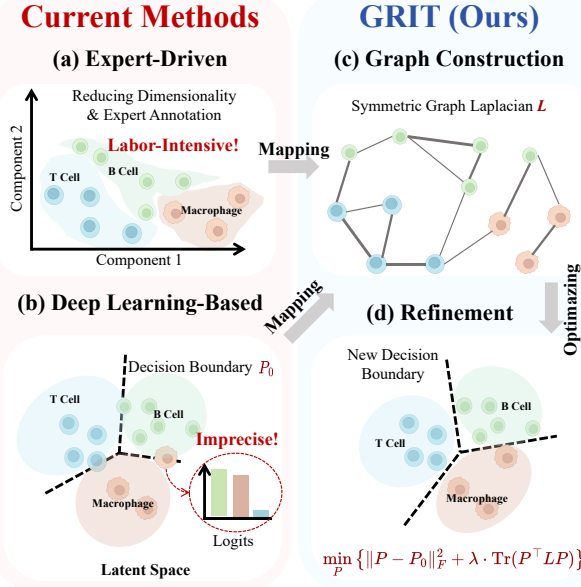


Figure 1: GRIT Overview. (a,b) Existing approaches rely on expert-driven labeling or deep learning models, which can be labor-intensive or imprecise. (c) Construct a PCA-based k -NN graph, with each node initialized by the logits predicted by a deep learning model. (d) GRIT refines these initial predictions by solving a graph-regularized optimization problem that promotes local consistency across the k -NN graph.

multimodal foundation models in other domains when trained at scale, there is strong reason to believe that such architectures—when further developed and trained on higher quality scRNA-seq and text corpora—can evolve into powerful tools for automating and augmenting expert-level biological annotation.

An important observation in the context of single-cell annotation is that human experts frequently rely on the structure revealed by the PCA-based k -NN graph. This suggests that, for a given scRNA-seq dataset, we already possess a reliable task-relevant structure among cells. While models like LangCell enable zero-shot annotation by aligning single-cell representations with natural language description representations, they are not explicitly trained to preserve this structural information. As a result, the predictions may be locally inconsistent with the k -NN graph which serves as an informative structural reference in expert-guided annotation workflows. This limitation motivates a hybrid strategy: refining pre-trained models’ zero-shot predictions by enforcing local consistency over the task-relevant k -NN graph. In doing so, we aim to combine the scalability provided by the pre-trained model with the structural robustness of the PCA-based k -NN graph. It is natural to consider existing methods such as label propagation or graph-based regularization. However, many of these approaches [39, 47, 48] require access to at least a subset of ground truth labels which are unavailable in the zero-shot setting. Others [2, 17, 38] focus on enhancing graph neural network training, which may be unnecessary in our case. These limitations call for a label-free, inference-time refinement approach tailored to the zero-shot annotation setting.

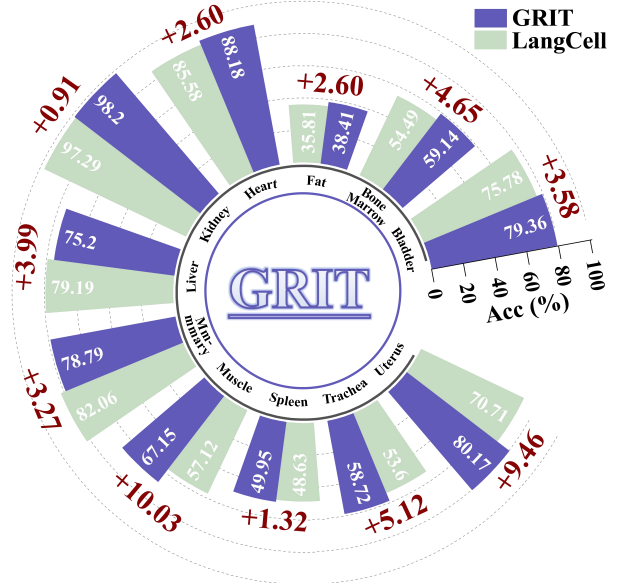


Figure 2: Performance of GRIT on zero-shot cell type annotation across 11 organ-specific scRNA-seq datasets. Each segment shows the accuracy achieved by GRIT (blue) and the baseline LangCell (green), along with the accuracy gain labeled in red. GRIT consistently improves performance over LangCell across all datasets, with accuracy gains up to 10%. Detailed results and analysis are provided in Section 4.2.

In this paper, we propose a graph-regularized logit refinement method (GRIT) for enhancing zero-shot cell type annotation in scRNA-seq data. The core idea is to leverage the scalability of pre-trained foundation models while correcting their predictions using domain-specific geometric consistency, without requiring any additional training (Figure 1). Concretely, we first apply a CLIP-style model—LangCell in our case—to perform zero-shot annotation on scRNA-seq data, resulting in initial prediction logits. We then construct a PCA-based k -NN graph to reflect the underlying structure commonly trusted by human experts. Finally, we solve a graph-regularized optimization problem to refine the logits, encouraging smoothness over the graph while remaining close to the original predictions. This refinement is applied entirely at inference time and serves as a lightweight, principled postprocessing step. We rigorously analyze our approach and validate its effectiveness through extensive experiments on 14 annotated human scRNA-seq datasets, collected from 4 independent studies and spanning 11 organs and over 200,000 single cells. Experimental results show that our refinement consistently improves zero-shot performance, with nearly all cases showing gains in accuracy and macro F1 score. Our main contributions are:

- We introduce a principled framework that integrates pre-trained foundation models with human expert annotation practices through inference-time graph regularization of prediction logits. Our method is simple, training-free, and effective, serving as a plug-and-play solution for zero-shot cell type annotation.

- We provide a theoretical proof that graph-regularized optimization can effectively refine predictions, under the condition the initial logits are reasonably accurate.
- Extensive zero-shot cell type annotation experiments using LangCell across 14 human scRNA-seq datasets demonstrate consistent performance improvements through the application of our graph-regularized logit refinement.

2 Related Work

2.1 Representation Learning for scRNA-seq

The increasing availability of single-cell RNA sequencing (scRNA-seq) data has spurred the development of machine learning approaches for learning meaningful representations from high dimensional gene expression profiles [12, 14, 16, 25, 26, 35, 37, 44, 49]. Traditional analysis pipelines often begin with dimensionality reduction techniques such as PCA or t-SNE, followed by clustering and manual marker gene inspection [5]. While these methods remain effective for visualizing structure and guiding expert annotation, recent work has turned to deep learning—particularly transformer-based architectures—to model complex nonlinear relationships across genes and enhance scalability to large, diverse datasets. Models such as scBERT[42], scGPT[7], GENEFORMER[8], and scFOUNDATION[11] leverage large-scale pretraining on millions of scRNA-seq profiles to support transfer learning across downstream tasks including cell type annotation.

2.2 Language-Cell Alignment and Zero-Shot Cell Type Annotation

Advances in multimodal representation learning aim to align heterogeneous data modalities within a shared semantic space, which is most prominently in the vision–language domain. A representative line of work demonstrates that contrastive or alignment-based pretraining can effectively bridge modality-specific representations with natural language supervision at scale. Concretely, general-purpose multimodal models such as CLIP [33], BLIP [19], LLaVA [20] and FLAMINGO [1], together with their domain-specific counterparts [15, 18, 24, 36, 40], demonstrate that aligning modality-specific encoders with large language models not only supports effective zero-shot transfer, but also enables instruction following and open-ended multimodal reasoning across diverse tasks.

Inspired by the success of these frameworks, recent work has begun to explore the alignment between cellular measurements and natural language. A representative example is LANGCELL [45], which introduces a CLIP-style contrastive pretraining framework to align scRNA-seq profiles with curated, ontology-derived textual descriptions. In this framework, GENEFORMER [8] is adopted as the cell encoder, while a BERT-based model is used for text encoding. While LangCell demonstrates promising generalization in zero-shot settings like zero-shot cell type annotations, several limitations remain. First, neither its cell encoder nor the multimodal model itself explicitly leverages graph-based structural information during pretraining. Second, its inference mechanism—like other CLIP-style retrieval paradigms [21, 23, 33]—can be sensitive to suboptimal prompt design and modality biases. We introduce a post-hoc logit refinement approach that exploits graph-structured consistency among cells to enhance prediction accuracy at inference time.

3 Methodology

In this section, we present our graph-regularized refinement method for enhancing zero-shot cell type annotation in scRNA-seq data. The core idea is to improve the initial prediction logits produced by a pretrained model via encouraging local consistency among cells, guided by structural information captured in a PCA-based k -NN graph. We begin by providing an analysis demonstrating that, when the initial logits are reasonably accurate, applying graph regularization is guaranteed to improve prediction performance. We then introduce the full pipeline of our proposed method, GRIT, for zero-shot cell type annotation.

3.1 Theoretical Analysis

THEOREM 1 (GRAPH REGULARIZED LOGIT REFINEMENT IMPROVES PREDICTIONS). *Given a symmetric graph Laplacian $L \in \mathbb{R}^{n \times n}$ constructed from an adjacency matrix $A \in \mathbb{R}^{n \times n}$, let $P_0 \in \mathbb{R}^{n \times c}$ denote the initial class logits over the n nodes, and let $P^* \in \mathbb{R}^{n \times c}$ denote the ground-truth logits. Consider the following graph-regularized optimization problem:*

$$\hat{P}_\lambda := \arg \min_P \{ \|P - P_0\|_F^2 + \lambda \cdot \text{Tr}(P^\top L P)\}.$$

Suppose the following condition holds:

$$\langle P_0 - P^*, L P_0 \rangle > 0.$$

Then there exists a sufficiently small regularization parameter $\lambda > 0$ such that:

$$\|\hat{P}_\lambda - P^*\|_F^2 < \|P_0 - P^*\|_F^2.$$

PROOF. The objective function is convex and quadratic, and the unique minimizer admits the closed-form solution:

$$\hat{P}_\lambda = (I + \lambda L)^{-1} P_0.$$

Define the function $f(\lambda) := \|\hat{P}_\lambda - P^*\|_F^2$. Since \hat{P}_λ is smooth in λ , $f(\lambda)$ is also continuously differentiable. At $\lambda = 0$, we have $\hat{P}_0 = P_0$, so:

$$f(0) = \|P_0 - P^*\|_F^2.$$

To study how $f(\lambda)$ changes near 0, compute the derivative using the chain rule. Let $A_\lambda := (I + \lambda L)^{-1}$, so $\hat{P}_\lambda = A_\lambda P_0$. Then:

$$\begin{aligned} f'(\lambda) &= \frac{d}{d\lambda} \|A_\lambda P_0 - P^*\|_F^2 \\ &= -2 \cdot \text{Tr} [(A_\lambda P_0 - P^*)^\top A_\lambda L A_\lambda P_0]. \end{aligned}$$

At $\lambda = 0$, we have $A_0 = I$, so:

$$\begin{aligned} f'(0) &= -2 \cdot \text{Tr} [(P_0 - P^*)^\top L P_0] \\ &= -2 \langle P_0 - P^*, L P_0 \rangle. \end{aligned}$$

By assumption, this quantity is strictly negative. Since $f(\lambda)$ is differentiable and $f'(0) < 0$, there exists some $\lambda > 0$ sufficiently small such that:

$$f(\lambda) < f(0),$$

i.e.,

$$\|\hat{P}_\lambda - P^*\|_F^2 < \|P_0 - P^*\|_F^2.$$

□

REMARK 1. The condition $\langle P_0 - P^*, LP_0 \rangle > 0$ captures a meaningful alignment between the prediction error and the graph structure. It implies that the residuals in P_0 are not arbitrary but exhibit disagreement that is structured according to the graph Laplacian. In other words, when a prediction is incorrect, its neighbors tend to disagree in directions that the regularizer penalizes. This condition is satisfied when P_0 is informative yet imperfect—e.g., capturing coarse structure but missing fine details. In such cases, the graph enables error correction by propagating reliable information across neighbors. This formalizes the intuition that logit refinement is effective when initial predictions are reasonable and graph reflects meaningful similarity.

3.2 The GRIT Method

We propose a three-stage framework GRIT for zero-shot cell type annotation in scRNA-seq data. Given an unlabeled dataset of n cells with gene expression profiles $\{x_i\}_{i=1}^n$ and a set of c cell type descriptions $\{t_j\}_{j=1}^c$, our method consists of: (1) obtaining initial logits via a CLIP-style model, (2) constructing a k -NN graph constructed in PCA space and (3) refining the initial logits using graph-regularized optimization (Figure 1).

Step 1: Initial Prediction via CLIP-Style Model. We first adopt a CLIP-style model, LangCell, to obtain the initial prediction logits $P_0 \in \mathbb{R}^{n \times c}$, where each row corresponds to a cell and each column to a candidate cell type. For each cell x_i , $P_0(i) = \text{model}(x_i, \{t_j\}_{j=1}^c)$, where $\text{model}(\cdot, \cdot)$ produces a probability distribution reflecting the alignment between the input cell and each cell type candidate. LangCell uses these logits for zero-shot prediction via: $g(x_i) = \arg \max_j \{P_0(i)\}$, $\forall i \in \{1, \dots, n\}$, enabling automatic cell type annotation without any task-specific training or fine-tuning. The logits P_0 serve as the input to our refinement procedure.

Step 2: Graph Construction. To model the relational structure among cells, we construct a k -NN graph based on a low-dimensional representation of the input data. Specifically, each cell x_i is first preprocessed following standard scRNA-seq analysis procedures. The resulting gene expression matrix is standardized and projected onto a d -dimensional space using principal component analysis (PCA), yielding a reduced representation x_i^{PCA} for each cell. Using these PCA-reduced features, we build a k -NN graph $\mathcal{G} = (\mathcal{V}, \mathcal{E})$ by connecting each cell to its k nearest neighbors in Euclidean space. The graph is symmetrized so that an undirected edge exists between cell i and cell j if either is among the k nearest neighbors of the other. Let $A \in \mathbb{R}^{n \times n}$ denote the adjacency matrix of this graph, the unnormalized graph Laplacian is then defined as $L = D - A$, where D is the diagonal degree matrix with $D_{ii} = \sum_j A_{ij}$. This Laplacian L captures the local geometry of the dataset and is used in the subsequent logit refinement step.

Step 3: Graph-regularized Logit Refinement. After obtaining the initial logits P_0 and the k -NN graph represented by the adjacency matrix A and its corresponding Laplacian L , we refine the logits by solving a graph-regularized optimization problem that promotes local consistency: $\hat{P}_\lambda = \arg \min_P \{\|P - P_0\|_F^2 + \lambda \text{Tr}(P^\top L P)\}$, where $\lambda > 0$ controls the strength of the regularization. This objective encourages the refined logits P to remain close to the initial predictions P_0 while being smooth with respect to the graph structure

encoded by L . The solution to this convex quadratic problem has a closed form and can be computed efficiently by solving a linear system: $\hat{P}_\lambda = (I + \lambda L)^{-1} P_0$. GRIT then uses the refined logits to perform zero-shot cell type annotation: $h(x_i) = \arg \max_j \{\hat{P}_\lambda(i)\}$.

4 Experiments

4.1 Datasets and Setup

We compile 11 scRNA-seq datasets from the *Tabula Sapiens* project [6], spanning organs including **Bladder**, **Bone Marrow**, **Fat**, **Heart**, **Kidney**, **Liver**, **Mammary**, **Muscle**, **Spleen**, **Trachea**, and **Uterus** (see Figure 3). In total, the datasets encompass 76 cell types and 171,383 single cells. In addition, we collect two public peripheral blood mononuclear cell datasets (**PBMC10k** [9] and **PBMC368k** [46]), and a peripheral cortex dataset (**Peripheral Cortex** [34]). These datasets cover 18 cell types and 33,700 single cells. All datasets include cell type annotations curated by domain experts. Dataset statistics is detailed in Appendix.

We focus on the zero-shot cell type annotation task on these datasets and employ LangCell, a pretrained CLIP model adapted for scRNA-seq and text alignment, to generate the initial soft label logits P_0 . Following standard preprocessing procedures in Scanpy [41] (see Appendix), a PCA-based k nearest neighbor (k -NN) graph is constructed for each dataset to capture cell similarity relationships. Unless otherwise stated, we use $\alpha = 0.2$ for LangCell, 50 principal components for PCA, and $k = 15$ for k -NN as our default hyperparameters. The initial logits P_0 are refined using GRIT with a default hyperparameter of $\lambda = 1$.

For comparison, we evaluate GRIT against LangCell and two intuitive baselines that directly combine the initial logits with the PCA-based k -NN graph. **(1) Majority Vote:** the predicted cell type is determined by the majority vote among the predictions of a cell and its neighbors $\arg \max_j \sum_{i' \in \mathcal{N}_k(i)} \mathbb{I}(g(x_{i'}) = j)$. **(2) Logit Average:** the logits of a cell and its neighbors are averaged to produce a refined logit, and the final prediction is obtained using the refined logit via $\arg \max_j \frac{1}{|\mathcal{N}_k(i)|} \sum_{i' \in \mathcal{N}_k(i)} P_0(i')$. Here we denote $\mathcal{N}_k(i)$ the set of k nearest neighbors of cell i in the PCA-based k -NN graph (including cell i itself). Performance of all methods is assessed using accuracy and macro F1 score (see Appendix), evaluating both overall and class-balanced predictive performance.

4.2 Main Results

Constructing a k -NN graph on principal components is a standard step in scRNA-seq analysis pipelines [10, 43]. It is common to reduce gene expression profiles to 50 principal components and set k to 15 or 20 when building the k -NN graph. For example, the widely used toolkits Scanpy [41] and Seurat [28] adopt 50 principal components by default, with $k = 15$ and $k = 20$, respectively. To align with established practice among domain experts, we evaluate GRIT under these commonly used configurations.

As shown in Table 1, GRIT consistently improves performance over the LangCell baseline across all 11 organ datasets, with accuracy improvements up to 10.03% (Muscle) and macro F1 improvements up to 4.62% (Liver) (see Appendix table for results with $k = 20$). Moreover, the results under $k = 15$ and $k = 20$ are similar, indicating strong robustness to the choice of k . Table 2 presents the logit consistency before and after GRIT refinement for both k

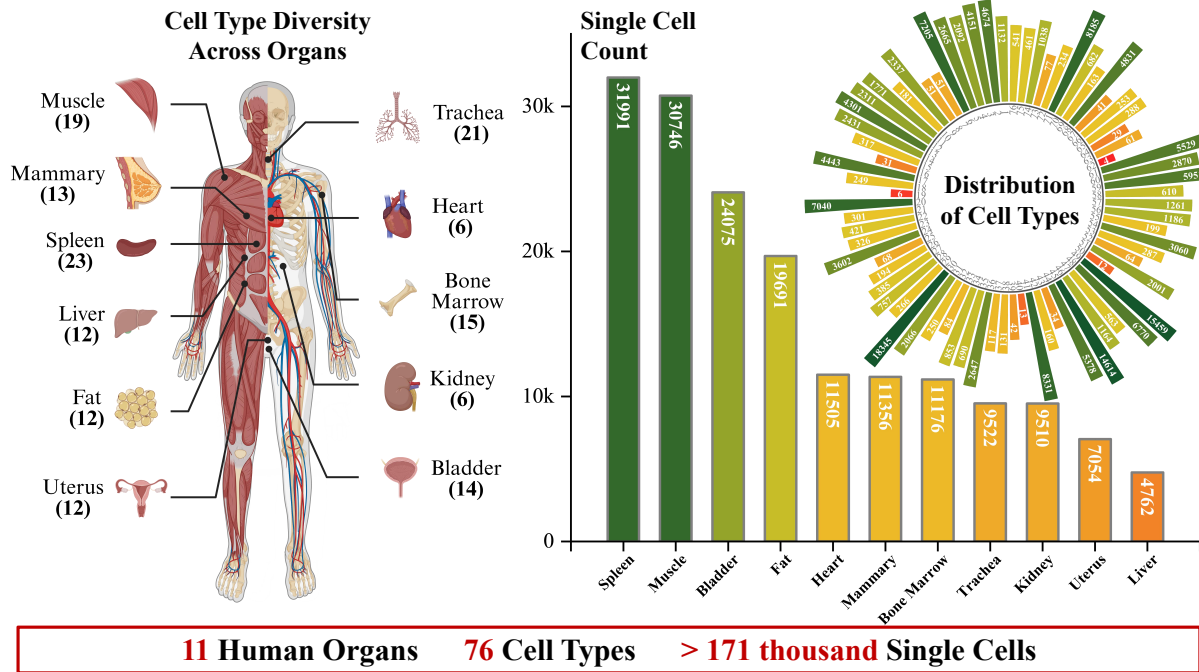


Figure 3: Overview of the human scRNA-seq datasets used in our main experiment. They span 11 human organs, 76 annotated cell types, and over 171,000 single cells. The anatomical illustration summarizes cell type diversity across organs. The bar chart reports single-cell counts per organ. The circular plot visualizes the distribution of all cell types, indexed from 1 to 76 for clarity. Full cell type names corresponding to these indices are listed in Appendix.

Table 1: Performance comparison on zero-shot cell type annotation across 11 scRNA-seq datasets from the *Tabula Sapiens* project. We evaluate LangCell, Majority Vote, Logit Average, and GRIT under the default hyperparameter setting, using Accuracy and Macro F1 (%). GRIT consistently outperforms the baseline LangCell across all datasets. The average row (Avg.) summarizes overall performance, with gains shown as colored subscripts.

Dataset	LangCell		Majority Vote		Logit Average		GRIT	
	Accuracy	Macro F1	Accuracy	Macro F1	Accuracy	Macro F1	Accuracy	Macro F1
Bladder	75.78	52.57	79.79 \uparrow	52.67 \uparrow	78.80 \uparrow	51.62 \downarrow	79.36 \uparrow	53.32 \uparrow
Bone Marrow	54.49	36.76	61.61 \uparrow	37.34 \uparrow	59.86 \uparrow	35.34 \downarrow	59.14 \uparrow	37.59 \uparrow
Fat	35.81	32.70	38.95 \uparrow	30.07 \downarrow	39.24 \uparrow	29.22 \downarrow	38.41 \uparrow	34.56 \uparrow
Heart	85.58	70.97	88.16 \uparrow	71.73 \uparrow	89.40 \uparrow	71.98 \uparrow	88.18 \uparrow	73.32 \uparrow
Kidney	97.29	84.60	93.85 \downarrow	52.59 \downarrow	93.55 \downarrow	50.73 \downarrow	98.20 \uparrow	85.03 \uparrow
Liver	75.20	52.23	77.89 \uparrow	48.84 \downarrow	77.99 \uparrow	48.27 \downarrow	79.19 \uparrow	56.85 \uparrow
Mammary	78.79	50.07	81.83 \uparrow	42.15 \downarrow	82.08 \uparrow	46.45 \downarrow	82.06 \uparrow	52.66 \uparrow
Muscle	57.12	31.35	70.61 \uparrow	32.09 \uparrow	72.60 \uparrow	31.79 \uparrow	67.15 \uparrow	35.50 \uparrow
Spleen	48.63	30.40	48.26 \downarrow	26.36 \downarrow	48.56 \downarrow	25.77 \downarrow	49.95 \uparrow	30.44 \uparrow
Trachea	53.60	39.34	61.65 \uparrow	37.38 \downarrow	61.36 \uparrow	37.25 \downarrow	58.72 \uparrow	40.34 \uparrow
Uterus	70.71	44.07	82.56 \uparrow	45.05 \uparrow	83.98 \uparrow	46.01 \uparrow	80.17 \uparrow	47.57 \uparrow
Avg.	66.64	47.73	71.38 $\uparrow_{4.74}$	43.30 $\downarrow_{4.43}$	71.58 $\uparrow_{4.94}$	43.13 $\downarrow_{4.60}$	70.96 $\uparrow_{4.32}$	49.74 $\uparrow_{2.01}$

settings, quantified by $P_0^T L P_0$ and $\hat{P}_\lambda^T L \hat{P}_\lambda$, respectively. GRIT consistently reduces logit inconsistency with respect to the graph structure, resulting in refined logits that better align with the k -NN graph used for cell type classification.

These findings support our central hypothesis that exploiting the k -NN graph structure—routinely employed by practitioners for

cell type annotation—enables meaningful refinement of the initial prediction logits produced by decent models, resulting in significant and stable improvements in predictive performance.

The refinement step solves a sparse linear system with a fixed coefficient matrix for each class using `scipy.sparse.linalg.spsolve`. Detailed computational cost are reported in Table 3. In particular,

Table 2: Logit consistency before and after the GRIT refinement across 11 organs. GRIT consistently reduces logit inconsistency with respect to the underlying graph structure.

Logit Consistency	Bladder	Bone Marrow	Fat	Heart	Kidney	Liver	Mammary	Muscle	Spleen	Trachea	Uterus
$P_0^T L P_0$ ($k = 15$)	60.54	25.10	40.09	35.85	44.41	15.58	29.32	81.48	58.48	17.94	17.67
$\hat{P}_\lambda^T L \hat{P}_\lambda$ ($k = 15$)	16.42	6.91	10.57	9.35	12.17	4.28	8.25	21.64	15.09	4.94	4.95
$P_0^T L P_0$ ($k = 20$)	60.98	25.37	40.28	36.01	44.62	15.67	29.70	82.21	58.71	18.07	17.79
$\hat{P}_\lambda^T L \hat{P}_\lambda$ ($k = 20$)	16.75	7.10	10.75	9.51	12.44	4.35	8.51	22.12	15.34	5.04	5.05

Table 3: Wall-clock time (minutes) required for GRIT graph regularization with $k=15$ and $k=20$ across the 11 datasets used in the main experiments, together with the number of cells (n) and the number of cell types (c) for each dataset.

-	Bladder	Bone Marrow	Fat	Heart	Kidney	Liver	Mammary	Muscle	Spleen	Trachea	Uterus
n	24,075	11,176	19,691	11,505	9,510	4,762	11,356	30,746	31,991	9,522	7,054
c	14	15	12	6	6	12	13	19	23	21	12
Clock-time ($k=15$)	0.76	0.11	0.33	0.18	1.06	0.03	0.12	10.27	5.79	0.20	0.11
Clock-time ($k=20$)	1.03	0.16	0.40	0.21	1.73	0.04	0.15	16.25	7.20	0.24	0.13

on the most computationally demanding dataset (Muscle, $n=30,746$, $c=19$), the default GRIT refinement completes in 10.27 ($k=15$) and 16.25 ($k=20$) minutes of wall-clock time.

We compare GRIT with two intuitive methods that directly combine the initial logits with the k -NN graph: Majority Vote and Logit Average. Although these approaches can increase prediction accuracy, they reduce the macro F1 score in more than half of all evaluated cases. Specifically, Majority Vote reduces the macro F1 on 6 out of 11 datasets for $k=15$ and on 8 out of 11 datasets for $k=20$. Logit Average reduces the macro F1 on 8 out of 11 datasets for $k=15$ and on 9 out of 11 datasets for $k=20$. This pattern indicates that such approaches tend to favor aggregate accuracy at the expense of class-wise performance balance, resulting in less balanced predictions. Notably, in the Kidney dataset, where the initial LangCell predictions are already strong (97.29% accuracy and 84.60% macro F1), both methods lead to substantial performance degradation. Majority Vote reduces accuracy to 93.85% (-3.44%) and macro F1 to 52.59% (-32.01%) for $k=15$, and to 93.88% (-3.41%) accuracy and 52.56% (-32.04%) macro F1 for $k=20$. Logit Averaging yields 93.55% (-3.74%) accuracy and 50.73% (-33.87%) macro F1 for $k=15$, and 93.62% (-3.67%) accuracy and 51.29% (-33.31%) macro F1 for $k=20$. This observation suggests that these heuristics are unstable and can be detrimental when the initial predictions are already of high quality.

4.3 Empirical Analysis of λ

In the Methodology section, we analyzed the behavior of the function $f(\lambda)$ which quantifies the quality of the refined logits \hat{P}_λ . Under a mild condition on the initial logits P_0 , we showed that $f(\lambda)$ decreases over a small right-hand interval near $\lambda=0$. Note that by definition, smaller values of $f(\lambda)$ correspond to higher-quality refined logits, whereas larger values indicate poorer-quality refinement. Motivated by this insight, we conduct a systematic sweep over λ values near zero. Specifically, we evaluate $\lambda \in \{10^{-5}, 10^{-4}, 10^{-3}, 10^{-2}, 0.1, 0.2, 0.5, 1, 2, 5, 10, 20, 30, 40, 50, 60, 70, 80, 90, 100\}$. Figure 4 (also see Appendix) illustrates how the prediction performance varies

Table 4: Performance comparison between LangCell and GRIT under varying α values and on additional datasets. We report Accuracy and Macro F1 (%). Arrows indicate relative performance of GRIT compared to LangCell.

Setting	LangCell		GRIT	
	Accuracy	Macro F1	Accuracy	Macro F1
$\alpha = 0.1$	63.60	46.01	66.87 \uparrow	47.66 \uparrow
$\alpha = 0.2$	66.59	47.73	70.96 \uparrow	49.74 \uparrow
$\alpha = 0.3$	67.39	48.32	71.48 \uparrow	49.78 \uparrow
$\alpha = 0.5$	67.05	48.27	70.65 \uparrow	49.47 \uparrow
PBMC10k	86.52	83.91	88.43 \uparrow	87.57 \uparrow
PBMC368k	84.86	83.17	87.41 \uparrow	86.16 \uparrow
Peripheral Cortex	98.01	72.87	98.41 \uparrow	73.27 \uparrow

with λ across all 11 human organ datasets, both individually and on average. Both the individual and average trend align with our analysis: performance improves as λ increases from zero. Empirically, we find that moderate values in the range $\lambda \in (0, 5)$ enhance the overall performance. We adopt $\lambda = 1$ as the default.

4.4 Robustness Across Different LangCell Hyperparameters and More Datasets

Our main experiments, along with empirical analysis in the low- λ regime, suggest that LangCell's zero-shot predictions are already sufficiently aligned with the graph structure for GRIT to provide effective improvements. To ensure a comprehensive evaluation, we further investigate a broader range of LangCell hyperparameter settings and datasets from studies in addition to the *Tabula Sapiens* project to assess generalizability across diverse input conditions.

As reported in LangCell, the hyperparameter $\alpha \in \{0.1, 0.2, 0.3, 0.5\}$ yields competitive results, with $\alpha = 0.2$ recommended as the default (see Appendix tables for details). We adopt $\alpha = 0.2$ for baseline comparisons, but also evaluate GRIT under all four α settings to

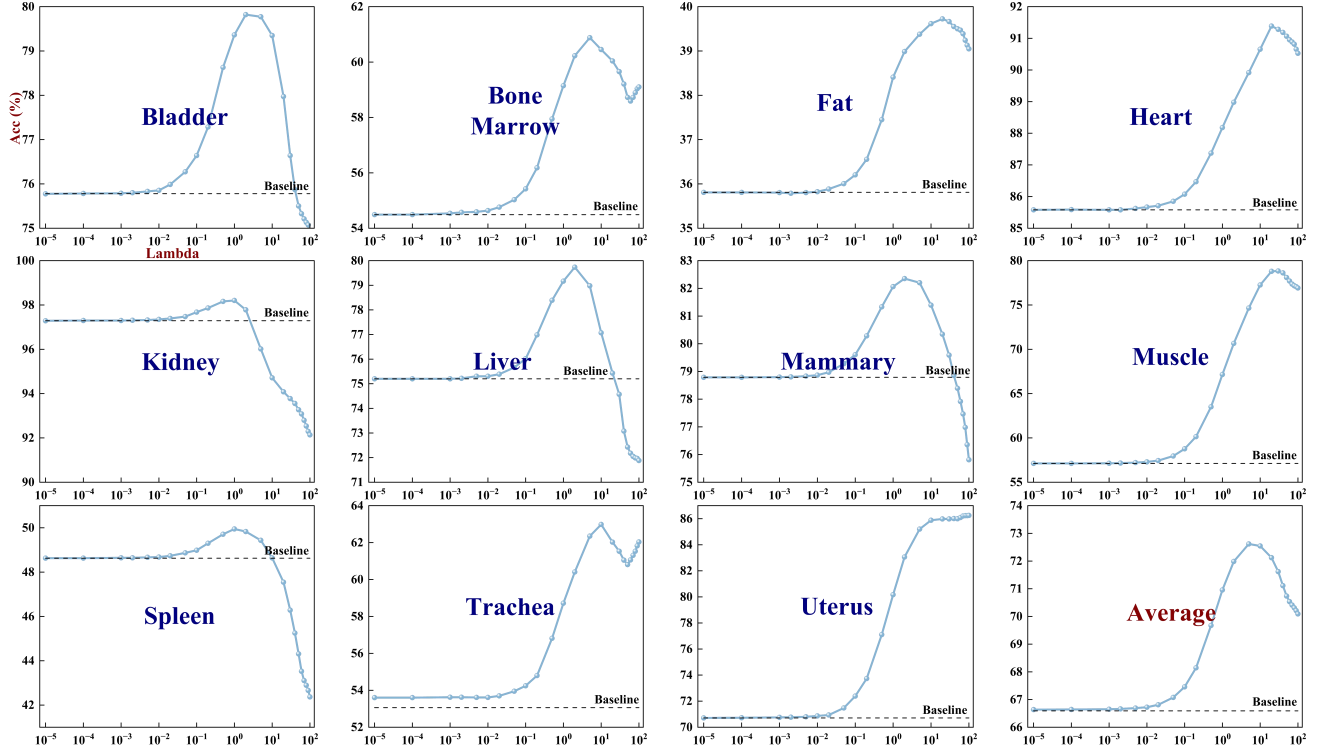


Figure 4: Investigation of GRIT performance in the right-hand neighborhood of $\lambda = 0$ across all 11 organs from the *Tabula Sapiens* project and their average. The x-axis denotes λ values, and the y-axis reports logit performance measured by accuracy. Dashed lines indicate baseline accuracies achieved by LangCell.

assess its robustness across a range of initializations. As shown in Table 4, GRIT consistently improves zero-shot annotation performance, measured by accuracy and macro F1, across all α values. These results underscore two key observations: (1) current zero-shot models like LangCell are capable of producing logits that already reflect a latent task-relevant structure, which can be effectively enhanced through graph-based refinement. (2) GRIT is robust to variations in initial logit quality, demonstrating consistent gains across a spectrum of strong configurations. Table 4 also presents GRIT’s performance on additional datasets including PBMC10k, PBMC368k, and Peripheral Cortex. GRIT consistently improves prediction performance across these datasets, demonstrating strong robustness to diverse data sources with varying levels of data noise.

4.5 Visualization and Case Study

We present three representative cases that exhibit clear performance improvements with GRIT, in order to illustrate the effect of the proposed refinement (Figure 5). In the UMAP visualizations, gray points denote correctly predicted cells, while green points indicate incorrectly predicted ones. As shown, the kidney dataset exhibits high initial prediction performance with LangCell, whereas the uterus and muscle datasets exhibit comparatively lower baseline accuracy. Nonetheless, across all cases, as long as a subset of correctly predicted cells exists within a local neighborhood, GRIT can propagate these signals to pull back mislabeled cells.

However, not all datasets benefit equally: in fat and spleen, GRIT slightly reduces macro F1 (see $k = 20$ results in Appendix). To further explore this trend, we analyze how GRIT improvement varies across various initial prediction qualities and dataset sizes. The improvement is visualized using color, where red indicates a significant performance gain, and green denotes a marginal improvement. Specifically, we examine initial accuracy, macro F1, and total cell count. As shown in Figure 6, GRIT tends to be more effective when the initial accuracy and macro F1 are relatively high. Additionally, when the initial performance is poor, large cell count number can degrade results. This observation is intuitive: reliable initial predictions ensure that neighbors provide trustworthy information, and a greater number of neighbors increases the likelihood of correcting noisy predictions through refinement. For noisy initial logits, the same propagation may reinforce incorrect patterns.

It is important to note that GRIT is not designed to achieve 100% accuracy. Rather, similar to other inference-time refinement methods [22, 31], it seeks to leverage complementary structural information in the data to bring the initial logits closer to their achievable performance limit. In our case, this is accomplished by promoting local consistency and semantic alignment with the k -NN graph. While the ultimate performance is bounded by the quality of the initial predictions, GRIT, like other inference-time refinement methods, introduces a principled and effective post hoc procedure that consistently yields measurable improvements.

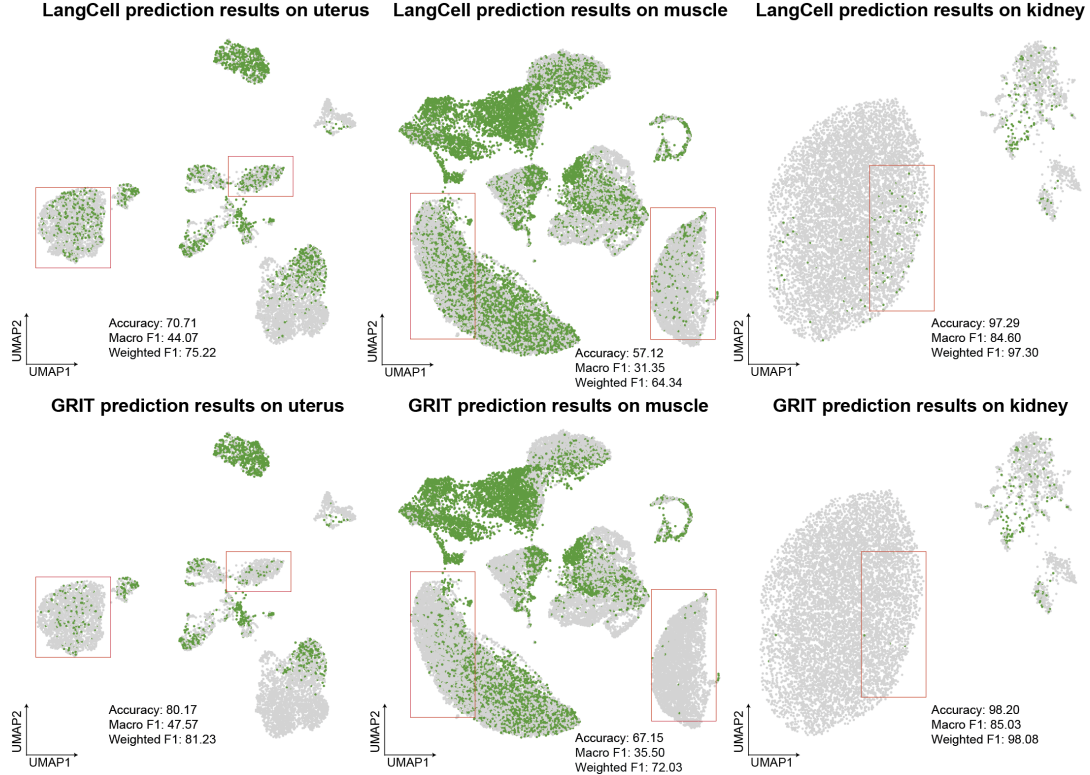


Figure 5: UMAP visualization of scRNA-seq data of organ uterus (left), muscle (middle), and kidney (right). Each point represents a cell, colored by prediction correctness: gray indicates correct predictions, and green indicates incorrect ones. For each organ, the top panel shows LangCell zero-shot predictions, the bottom panel shows refined predictions from GRIT. Orange boxes indicate representative regions where GRIT provides clear improvements.

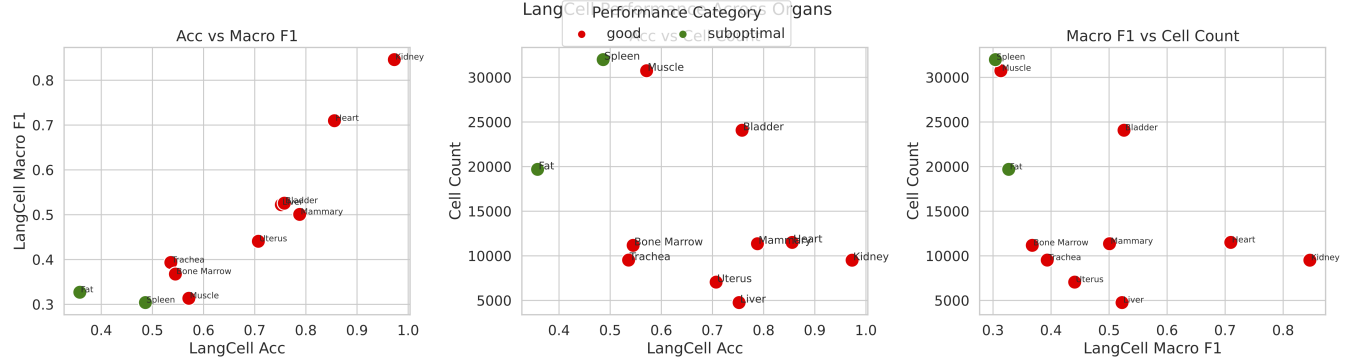


Figure 6: GRIT performance are plotted against LangCell logit initial accuracy, macro F1, and total cell count for all 11 scRNA-seq datasets used in our main experiment.

5 Limitations and Ethical Considerations

All experiments in this work are conducted on publicly available and de-identified datasets that were released for research use. We do not collect new data, nor do we have access to any personally identifiable information. Informed consent was obtained by the original data collectors, and no additional consent procedures are required for this study. Accordingly, this study does not involve direct interaction with human participants.

6 Conclusion

We present GRIT, a biologically grounded, training-free refinement method for improving zero-shot cell type annotation in scRNA-seq data. GRIT is designed to be as a principled, plug-in post-processing step that can be applied to any pretrained model producing cell-level logits. While effective, GRIT assumes a reliable graph and reasonably accurate initial logits. Future works include developing adaptive λ selection strategies and extending GRIT to multi-omics.

7 GenAI Disclosure

Generative AI tools were used in a limited capacity during the preparation of this manuscript, primarily for language polishing and minor editorial assistance. All methodological designs, algorithmic formulations, experimental analyses, and conclusions were conceived, implemented, and verified by the authors. The use of generative AI did not influence the reported results.

References

- [1] Jean-Baptiste Alayrac, Jeff Donahue, Pauline Luc, Antoine Miech, Iain Barr, Yana Hasson, Karel Lenc, Arthur Mensch, Katherine Millican, Malcolm Reynolds, et al. 2022. Flamingo: a visual language model for few-shot learning. *Advances in neural information processing systems* 35 (2022), 23716–23736.
- [2] Fuqun Chen, Guanhua Zou, Yongxian Wu, and Le Ou-Yang. 2024. Clustering single-cell multi-omics data via graph regularized multi-view ensemble learning. *Bioinformatics* 40, 4 (2024), btae169.
- [3] Li-Fang Chu and et al. 2016. Single-cell RNA-seq reveals novel regulators of human embryonic stem cell differentiation to definitive endoderm. *Genome Biology* 17 (2016), 173. doi:10.1186/s13059-016-1033-x
- [4] Zoe A Clarke, Tallulah S Andrews, Jawairia Atif, Delaram Pouyabahar, Brendan T Innes, Sonya A MacParland, and Gary D Bader. 2021. Tutorial: guidelines for annotating single-cell transcriptomic maps using automated and manual methods. *Nature protocols* 16, 6 (2021), 2749–2764.
- [5] Ashley Mae Conard, Alan DenAdel, and Lorin Crawford. 2023. A spectrum of explainable and interpretable machine learning approaches for genomic studies. *Wiley Interdisciplinary Reviews: Computational Statistics* 15, 5 (2023), e1617.
- [6] The Tabula Sapiens Consortium*, Robert C Jones, Jim Karkanas, Mark A Krasnow, Angela Oliveira Pisco, Stephen R Quake, Julia Salzman, Nir Yosef, Bryan Bulthaupt, Phillip Brown, et al. 2022. The Tabula Sapiens: A multiple-organ, single-cell transcriptomic atlas of humans. *Science* 376, 6594 (2022), eab14896.
- [7] Haotian Cui, Chloe Wang, Hassaan Maan, Kuan Pang, Fengning Luo, Nan Duan, and Bo Wang. 2024. scGPT: toward building a foundation model for single-cell multi-omics using generative AI. *Nature Methods* 21, 8 (2024), 1470–1480.
- [8] Zhanbei Cui, Tongda Xu, Jia Wang, Yu Liao, and Yan Wang. 2024. Geneformer: Learned gene compression using transformer-based context modeling. In *ICASSP 2024-2024 IEEE International Conference on Acoustics, Speech and Signal Processing (ICASSP)*. IEEE, 8035–8039.
- [9] Adam Gayoso, Romain Lopez, Galen Xing, Pierre Boyreau, Valeh Valiollah Pour Amiri, Justin Hong, Katherine Wu, Michael Jayasuriya, Edouard Mehlman, Maxime Langevin, et al. 2022. A Python library for probabilistic analysis of single-cell omics data. *Nature biotechnology* 40, 2 (2022), 163–166.
- [10] Gongde Guo, Hui Wang, David Bell, Yixin Bi, and Kieran Greer. 2003. KNN model-based approach in classification. In *On The Move to Meaningful Internet Systems 2003: CoopIS, DOA, and ODBASE: OTM Confederated International Conferences, CoopIS, DOA, and ODBASE 2003, Catania, Sicily, Italy, November 3-7, 2003. Proceedings*. Springer, 986–996.
- [11] Minsheng Hao, Jing Gong, Xin Zeng, Chiming Liu, Yucheng Guo, Xingyi Cheng, Taifeng Wang, Jianzhu Ma, Xuegong Zhang, and Le Song. 2024. Large-scale foundation model on single-cell transcriptomics. *Nature methods* 21, 8 (2024), 1481–1491.
- [12] Ashraful Haque, Jessica Engel, Sarah A Teichmann, and Tapio Lönnerberg. 2017. A practical guide to single-cell RNA-sequencing for biomedical research and clinical applications. *Genome medicine* 9 (2017), 1–12.
- [13] Congxue Hu, Tengye Li, Yingqi Xu, Xinxin Zhang, Feng Li, Jing Bai, Jing Chen, Wenqi Jiang, Kaiyu Yang, Qi Ou, et al. 2023. CellMarker 2.0: an updated database of manually curated cell markers in human/mouse and web tools based on scRNA-seq data. *Nucleic acids research* 51, D1 (2023), D870–D876.
- [14] Byungjin Hwang, Ji Hyun Lee, and Duhee Bang. 2018. Single-cell RNA sequencing technologies and bioinformatics pipelines. *Experimental & molecular medicine* 50, 8 (2018), 1–14.
- [15] Songtao Jiang, Yuan Wang, Sibo Song, Tianxiang Hu, Chenyi Zhou, Bin Pu, Yan Zhang, Zhibo Yang, Yang Feng, Joey Tianyi Zhou, et al. 2025. Hulu-med: A transparent generalist model towards holistic medical vision-language understanding. *arXiv preprint arXiv:2510.08668* (2025).
- [16] Dragomirka Jovic, Xue Liang, Hua Zeng, Lin Lin, Fengping Xu, and Yonglun Luo. 2022. Single-cell RNA sequencing technologies and applications: A brief overview. *Clinical and translational medicine* 12, 3 (2022), e694.
- [17] TN Kipf. 2016. Semi-Supervised Classification with Graph Convolutional Networks. *arXiv preprint arXiv:1609.02907* (2016).
- [18] Chunyuan Li, Cliff Wong, Sheng Zhang, Naoto Usuyama, Haotian Liu, Jianwei Yang, Tristan Naumann, Hoifung Poon, and Jianfeng Gao. 2023. Llava-med: Training a large language-and-vision assistant for biomedicine in one day. *Advances in Neural Information Processing Systems* 36 (2023), 28541–28564.
- [19] Junnan Li, Dongxu Li, Caiming Xiong, and Steven Hoi. 2022. Blip: Bootstrapping language-image pre-training for unified vision-language understanding and generation. In *International conference on machine learning*. PMLR, 12888–12900.
- [20] Haotian Liu, Chunyuan Li, Qingyang Wu, and Yong Jae Lee. 2023. Visual instruction tuning. *Advances in neural information processing systems* 36 (2023), 34892–34916.
- [21] Jiaxiang Liu, Tianxiang Hu, Jiawei Du, Ruiyuan Zhang, Joey Tianyi Zhou, and Zuozhu Liu. 2025. KPL: Training-Free Medical Knowledge Mining of Vision-Language Models. *Proceedings of the AAAI Conference on Artificial Intelligence* 39, 18 (2025), 18852–18860.
- [22] Jiaxiang Liu, Tianxiang Hu, Jiawei Du, Ruiyuan Zhang, Joey Tianyi Zhou, and Zuozhu Liu. 2025. Kpl: Training-free medical knowledge mining of vision-language models. In *Proceedings of the AAAI Conference on Artificial Intelligence*, Vol. 39. 18852–18860.
- [23] Jiaxiang Liu, Tianxiang Hu, Huimin Xiong, Jiawei Du, Yang Feng, Jian Wu, Joey Zhou, and Zuozhu Liu. 2024. Vpl: Visual proxy learning framework for zero-shot medical image diagnosis. In *Findings of the Association for Computational Linguistics: EMNLP 2024*. 9978–9992.
- [24] Michael Moor, Qian Huang, Shirley Wu, Michihiro Yasunaga, Yash Dalmia, Jure Leskovec, Cyril Zakka, Eduardo Pontes Reis, and Pranav Rajpurkar. 2023. Medflamingo: a multimodal medical few-shot learner. In *Machine Learning for Health (ML4H)*. PMLR, 353–367.
- [25] Thale Kristin Olsen and Ninib Baryawno. 2018. Introduction to single-cell RNA sequencing. *Current protocols in molecular biology* 122, 1 (2018), e57.
- [26] Eftymia Papalexi and Rahul Satija. 2018. Single-cell RNA sequencing to explore immune cell heterogeneity. *Nature Reviews Immunology* 18, 1 (2018), 35–45.
- [27] Giovanni Pasquini, Jesus Eduardo Roja Arias, Patrick Schäfer, and Volker Busskamp. 2021. Automated methods for cell type annotation on scRNA-seq data. *Computational and Structural Biotechnology Journal* 19 (2021), 961–969.
- [28] Wendell J Pereira, Felipe Marques Almeida, D Conde, KM Balmant, PM Triozzi, HW Schmidt, C Dervinis, CJ Pappas, and M Kirst. 2021. Asc-Seurat: analytical single-cell Seurat-based web application. *BMC bioinformatics* 22 (2021), 1–14.
- [29] Hannah A Pliner, Jay Shendure, and Cole Trapnell. 2019. Supervised classification enables rapid annotation of cell atlases. *Nature methods* 16, 10 (2019), 983–986.
- [30] Alex A. Pollen and et al. 2015. Molecular identity of human outer radial glia during cortical development. *Cell* 163 (2015), 55–67. doi:10.1016/j.cell.2015.09.004
- [31] Qi Qian, Yuanhong Xu, and Juhua Hu. 2023. Intra-modal proxy learning for zero-shot visual categorization with clip. *Advances in Neural Information Processing Systems* 36 (2023), 25461–25474.
- [32] Fei Quan, Xin Liang, Mingjiang Cheng, Huan Yang, Kun Liu, Shengyuan He, Shangqin Sun, Menglan Deng, Yanzhen He, Wei Liu, et al. 2023. Annotation of cell types (ACT): a convenient web server for cell type annotation. *Genome Medicine* 15, 1 (2023), 91.
- [33] Alex Radford, Jong Wook Kim, Chris Hallacy, Aditya Ramesh, Gabriel Goh, Sandhini Agarwal, Girish Sastry, Amanda Askell, Pamela Mishkin, Jack Clark, et al. 2021. Learning transferable visual models from natural language supervision. In *International conference on machine learning*. PMLR, 8748–8763.
- [34] Kimberly Siletti, Rebecca Hodge, Alejandro Mossi Albiach, Ka Wai Lee, Song-Lin Ding, Lijuan Hu, Peter Lönnerberg, Trygve Bakken, Tamara Casper, Michael Clark, et al. 2023. Transcriptomic diversity of cell types across the adult human brain. *Science* 382, 6667 (2023), eadd7046.
- [35] Shaked Slovin, Annamaria Carissimo, Francesco Panariello, Antonio Grimaldi, Valentina Bouché, Gennaro Gambardella, and Davide Cacchiarelli. 2021. Single-cell RNA sequencing analysis: a step-by-step overview. *RNA bioinformatics* (2021), 343–365.
- [36] Samuel Stevens, Jiaman Wu, Matthew J Thompson, Elizabeth G Campolongo, Chan Hee Song, David Edward Carlyn, Li Dong, Wasila M Dahdul, Charles Stewart, Tanya Berger-Wolf, et al. 2024. Bioclip: A vision foundation model for the tree of life. In *Proceedings of the IEEE/CVF conference on computer vision and pattern recognition*. 19412–19424.
- [37] Bram Van de Sande, Joon Sang Lee, Euphemia Mutasa-Gottgens, Bart Naughton, Wendi Bacon, Jonathan Manning, Yong Wang, Jack Pollard, Melissa Mendez, Jon Hill, et al. 2023. Applications of single-cell RNA sequencing in drug discovery and development. *Nature Reviews Drug Discovery* 22, 6 (2023), 496–520.
- [38] Petar Veličković, William Fedus, William L Hamilton, Pietro Liò, Yoshua Bengio, and R Devon Hjelm. 2018. Deep graph infomax. *arXiv preprint arXiv:1809.10341* (2018).
- [39] Hongwei Wang, Fuzheng Zhang, Mengdi Zhang, Jure Leskovec, Miao Zhao, Wenjie Li, and Zhongyuan Wang. 2019. Knowledge-aware graph neural networks with label smoothness regularization for recommender systems. In *Proceedings of the 25th ACM SIGKDD international conference on knowledge discovery & data mining*. 968–977.
- [40] Zifeng Wang, Zhenbang Wu, Dinesh Agarwal, and Jimeng Sun. 2022. Medclip: Contrastive learning from unpaired medical images and text. In *Proceedings of the Conference on Empirical Methods in Natural Language Processing. Conference on Empirical Methods in Natural Language Processing*, Vol. 2022. 3876.
- [41] F Alexander Wolf, Philipp Angerer, and Fabian J Theis. 2018. SCANPY: large-scale single-cell gene expression data analysis. *Genome biology* 19 (2018), 1–5.

- [42] Fan Yang, Wenchuan Wang, Fang Wang, Yuan Fang, Duyu Tang, Junzhou Huang, Hui Lu, and Jianhua Yao. 2022. scBERT as a large-scale pretrained deep language model for cell type annotation of single-cell RNA-seq data. *Nature Machine Intelligence* 4, 10 (2022), 852–866.
- [43] Shichao Zhang, Xuelong Li, Ming Zong, Xiaofeng Zhu, and Debo Cheng. 2017. Learning k for knn classification. *ACM Transactions on Intelligent Systems and Technology (TIST)* 8, 3 (2017), 1–19.
- [44] Yijie Zhang, Dan Wang, Miao Peng, Le Tang, Jiawei Ouyang, Fang Xiong, Can Guo, Yanyan Tang, Yujuan Zhou, Qianjin Liao, et al. 2021. Single-cell RNA sequencing in cancer research. *Journal of Experimental & Clinical Cancer Research* 40 (2021), 1–17.
- [45] Suyuan Zhao, Jiahuan Zhang, Yushuai Wu, Yizhen Luo, and Zaiqing Nie. 2024. LangCell: Language-Cell Pre-training for Cell Identity Understanding. In *International Conference on Machine Learning*. PMLR, 61159–61185.
- [46] Grace XY Zheng, Jessica M Terry, Phillip Belgrader, Paul Ryvkin, Zachary W Bent, Ryan Wilson, Solongo B Ziraldo, Tobias D Wheeler, Geoff P McDermott, Junjie Zhu, et al. 2017. Massively parallel digital transcriptional profiling of single cells. *Nature communications* 8, 1 (2017), 14049.
- [47] Dengyong Zhou, Olivier Bousquet, Thomas Lal, Jason Weston, and Bernhard Schölkopf. 2003. Learning with local and global consistency. *Advances in neural information processing systems* 16 (2003).
- [48] Xiaojin Zhu, Zoubin Ghahramani, and John D Lafferty. 2003. Semi-supervised learning using gaussian fields and harmonic functions. In *Proceedings of the 20th International conference on Machine learning (ICML-03)*. 912–919.
- [49] Christoph Ziegenhain, Beate Vieth, Swati Parekh, Björn Reinius, Amy Guillaumet-Adkins, Martha Smets, Heinrich Leonhardt, Holger Heyn, Ines Hellmann, and Wolfgang Enard. 2017. Comparative analysis of single-cell RNA sequencing methods. *Molecular cell* 65, 4 (2017), 631–643.